NSRRC - Jou980 (2015)

CellPress

Structure
Article

Solution Structure of Apoptotic BAX Oligomer: Oligomerization Likely Precedes Membrane Insertion

Tai-Ching Sung,[1] Ching-Yu Li,[1] Yei-Chen Lai,[1] Chien-Lun Hung,[1] Orion Shih,[2] Yi-Qi Yeh,[2] U-Ser Jeng,[2] and Yun-Wei Chiang[1,*]
[1]Department of Chemistry, National Tsing Hua University, Hsinchu 30013, Taiwan
[2]National Synchrotron Radiation Research Center, Hsinchu 30076, Taiwan
*Correspondence: ywchiang@mx.nthu.edu.tw
http://dx.doi.org/10.1016/j.str.2015.07.013

SUMMARY

Proapoptotic BAX protein is largely cytosolic in healthy cells, but it oligomerizes and translocates to mitochondria upon receiving apoptotic stimuli. A long-standing challenge has been the inability to capture any structural information beyond the onset of activation. Here, we present solution structures of an activated BAX oligomer by means of spectroscopic and scattering methods, providing details about the monomer-monomer interfaces in the oligomer and how the oligomer is assembled from homodimers. We show that this soluble oligomer undergoes a direct conversion into membrane-inserted oligomer, which has the ability of inducing apoptosis and structurally resembles a membrane-embedded oligomer formed from BAX monomers in lipid environment. Structural differences between the soluble and the membrane-inserted oligomers are manifested in the C-terminal helices. Our data suggest an alternative pathway of apoptosis in which BAX oligomer formation occurs prior to membrane insertion.

INTRODUCTION

Bcl-2 associated X (BAX) is a member of the Bcl-2 protein family, acting as a central gatekeeper that controls apoptotic signaling between cytosol and mitochondria in the Bcl-2-mediated apoptosis (Moldoveanu et al., 2014; Suzuki et al., 2000; Youle and Strasser, 2008). In healthy cells, BAX is located primarily in cytosol. Upon receipt of apoptotic signaling, BAX undergoes conformational changes and oligomerization, eventually becoming a membrane-associated complex, causing the BAX-induced mitochondrial outer membrane permeabilization (MOMP) event (Häcker and Weber, 2007; Youle and Strasser, 2008). Accumulating evidence has demonstrated the oligomerization of BAX proteins and its essential roles in apoptosis; however, it remains unclear about which mechanism BAX is triggered to become active to initiate the translocation from cytosol to mitochondria, thereby leading to the apoptosis (Antonsson et al., 2000; Czabotar et al., 2013; Dejean et al., 2005). This pivotal step remains poorly understood, largely because little is known about the structure of the activated forms of full-length BAX in the process. Crystal structures of the activated BAX were reported previously, but only available in forms of truncated BAX fragments (Czabotar et al., 2013). Some recent studies, based on dimer forms of membrane-embedded BAX, have reported that an important structural change after the BAX activation is the opening of the hairpin formed by helices 5 and 6, but there remains uncertainty concerning the structures of the activated BAX oligomer (Bleicken et al., 2014; Westphal et al., 2014). It is not known whether the formation of BAX oligomers occurs prior to or at the moment of its interaction with mitochondria (Cartron et al., 2008; Dejean et al., 2005). A complete view about the mechanisms implicated in the insertion of BAX into mitochondria is yet to be explored.

Seeking structural clues into the mechanism of BAX-induced MOMP activity, we undertook structural studies of soluble activated BAX proteins using molecular modeling and experimental methods including electron spin resonance (ESR) and small-angle X-ray scattering (SAXS). Basically, nitroxide side chain (designated as R1) is attached covalently to a cysteine introduced on a BAX protein through site-specific mutagenesis. As a result, information on local environment, dynamics, and inter-spin-label distances can be conveniently obtained by studying the ESR spectrum of R1 (Airola et al., 2013; Georgieva et al., 2013; Jeschke, 2012; López et al., 2013; Pliotas et al., 2012). Here, we present solution structural models of the activated BAX monomer, dimer, and tetramer in an apoptotic oligomer state induced by BimBH3 peptides (Gavathiotis et al., 2008, 2010; Tsai et al., 2015), we demonstrate structural arrangement of the core domain (helices 2 to 6) within the dimer unit consistent with a long-standing model, and we build a tetramer model for the activated BAX to provide structural insights into the assemblies of BAX dimers, suggesting an alternative pathway of the BAX-mediated apoptosis.

RESULTS

Interspin Distance Measurements by ESR

Figure 1A shows the structure of inactive BAX monomer and the mutation sites used in the present study. As indicated, the spin-labeled sites cover all of the nine helices of BAX. A double electron-electron resonance (DEER) experiment was carried out to measure distances between spin labels for doubly labeled BAX (with spin dilution of 1:1 labeled/unlabeled mixtures) and singly labeled BAX, all of which are in the BimBH3-induced oligomer state. The soluble oligomers were induced by incubation with

 ©2015 Elsevier Ltd All rights reserved
CrossMark

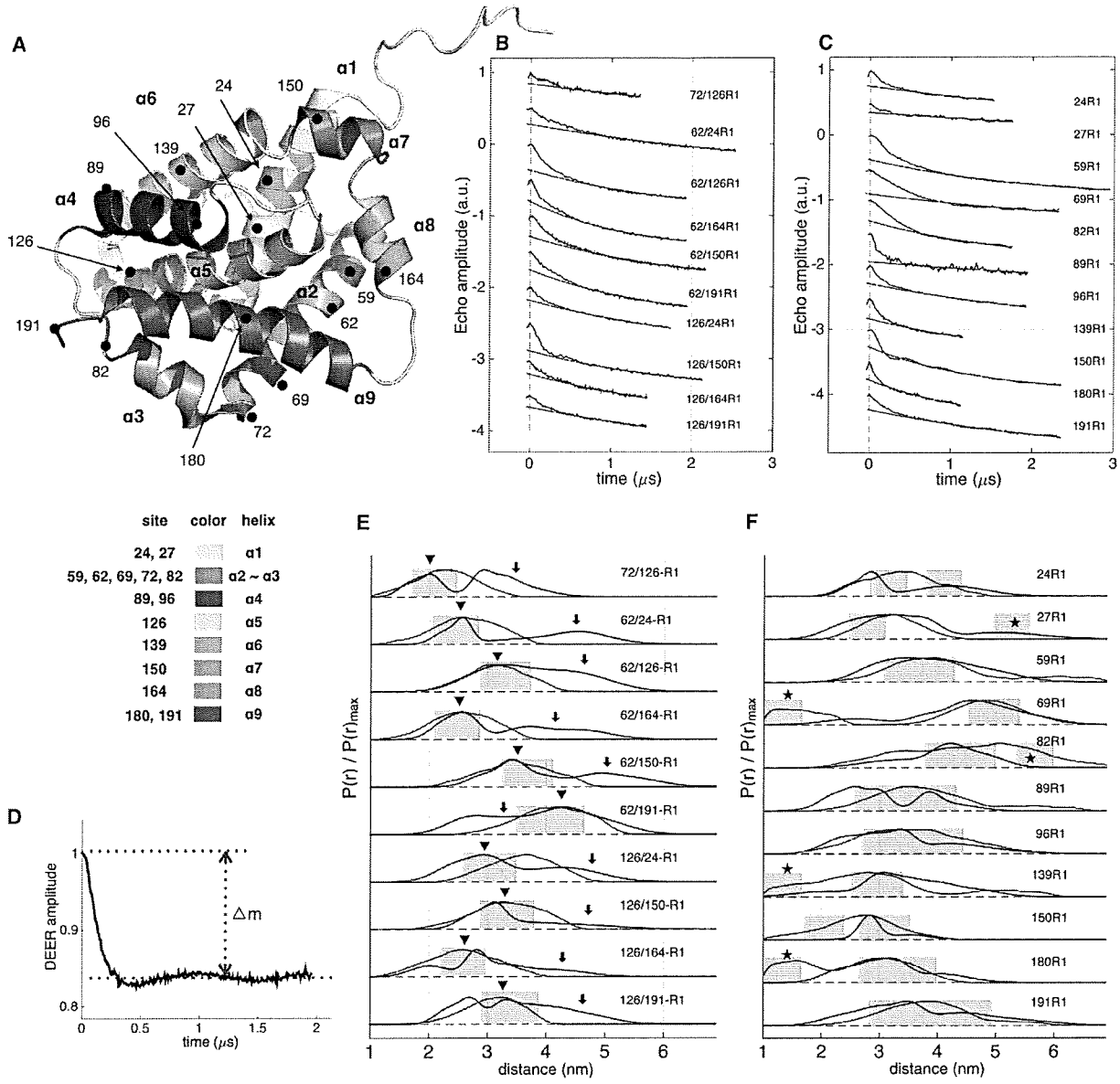

Figure 1. Spin-Labeling Sites and Distance Measurements

(A) Structure of inactive BAX monomer (PDB: 1F16) and mutation sites used for spin-labeling study. Raw time-domain DEER data (blue lines) for (B) double-labeled and (C) single-labeled BAX O mutants. Background traces of the time-domain data are shown in red.

(D) Illustration of modulation depth of time-domain DEER.

(E) Distance distributions P(r) extracted from the DEER measurements of doubly labeled BAX oligomers (with spin dilution) using TIKR method. The TIKR-P(r) results (blue) were used to derive the structure of activated BAX monomer. Predictions for the intramonomer distances by MtsslWizard (gray shaded area) and MMM (red) programs are in a good agreement with the TIKR-P(r) peaks assigned to interlabel distances within the activated monomer (denoted by triangles). Peaks corresponding to intermonomer distances are denoted by arrows and discussed in later sections.

(F) TIKR-P(r) results (blue) from singly labeled BAX oligomers. Predictions from the MtsslWizard and MMM calculations were made based on the tetramer model derived from the TIKR results. The model calculations fit nicely to the TIKR-P(r), except a few discrepancies (indicated by stars) caused by the limitation of DEER measurements. See also Figure S1.

BimBH3 peptides and purified by size-exclusion chromatography (SEC) fast protein liquid chromatography (FPLC) in the absence of membranes (see Experimental Procedures). Figures 1B and 1C show raw time-domain DEER data (blue lines) of the studied BAX mutants. The time-domain DEER data after baseline subtraction are shown in Figure S1A. Modulation depth (Δm; see Figure 1D) of DEER data was previously demonstrated (Bode et al., 2007) to count the number of coupled spins

(in a sphere of 6-nm radius, approximately), <N>. The <N> value was found to be 2.78 (with SD $\sigma\sim$ 0.66) and 3.35 ($\sigma\sim$ 0.72) for the doubly labeled (with spin dilution) and singly labeled BAX mutants, respectively, from the DEER data. Details of the analysis are given in Supplemental Experimental Procedures. Perhaps the most important point arising from the analysis is that more than two coupled spins were collected in the measurements. A careful procedure to distinguish desired from undesired spin-pairs in the oligomer is needed and the details are given below.

Peak Assignment for the Distance Distributions

The time-domain DEER data were analyzed using the Tikhonov regularization (TIKR) method (Chiang et al., 2005) to yield inter-spin distance distributions P(r). Figure 1E (blue lines) shows the obtained TIKR-P(r) for the doubly labeled BAX oligomers. The TIKR-P(r) results are clearly characterized by multiple peaks, exhibiting heterogeneity, in line with the result of the modulation depth analysis. The heterogeneity is confirmed to be caused by various inter- and intramonomer distances rather than numerical artifacts using the approach demonstrated in Figures S2A–B. A self-consistent iteration (SCI) strategy (details in Supplemental Experimental Procedures and Figure S2C) was then implemented so as to determine the structures of the activated BAX monomer (i.e., the monomer unit within the BAX oligomer), dimer, tetramer, and oligomer. Our results show that the activated oligomer is assembled from BAX dimers. For simplicity of presentation, we first describe the P(r) results (Figures 1E and 1F) and then give details of the determined structures in later sections. During the SCI procedure, we generated many plausible structural models using PyMOL and then checked on the derived structural models using two different modeling programs, MtsslWizard and multiscale modeling of macromolecules (MMM) (Hagelueken et al., 2012; Polyhach et al., 2011). Predictions (from the two modeling programs) for the intramonomer distances within the determined oligomer structure are displayed in red lines and the gray shaded area (Figure 1E), showing good agreement with each other. Most importantly, the modeling predictions are consistent with those peaks (denoted by triangles in Figure 1E) in the TIKR-P(r) results that were assigned to intramonomer distances within an oligomer. This result provides support for the model of the activated BAX monomer derived from the TIKR results (details given in Table S1). Other peaks (denoted by arrows in Figure 1E) that were not fitted by the simulated intramonomer P(r) were verified to be caused by intermonomer distances within the oligomer. The verification was performed by MMM model calculations (Figure S2C) excluding the intramonomer distances.

Figure 1F shows results of the singly labeled BAX oligomers. The TIKR-P(r) results (blue lines) provide intermonomeric information enabling the reconstruction of an oligomer model using the activated monomer model determined from the study of Figure 1E. Therefore, the TIKR-P(r) results (Figure 1F) were used for molecular docking (also performed with MtsslWizard and MMM programs) to reconstruct models of BAX dimer and tetramer during the SCI procedure. The predictions (red lines in Figure 1F) from the MMM and MtsslWizard programs were made based on the reconstructed tetramer model and achieved a satisfactory fit, with few exceptions (denoted by stars in Figure 1F), to the TIKR-P(r). The exceptions were a result of the limitations of the experimental setup used. Our DEER measurement was most sensitive to distances in the range of 1.5–6 nm.

Activated Monomer and Dimer Structures within an Oligomer

Figure 2A shows the determined structure of the activated monomer embedded in an oligomer. The activated monomer is substantially different in conformation compared with the inactive BAX (Figure 1A). Our molecular docking analysis (see Supplemental Experimental Procedures) indicates that the oligomer is assembled from BAX dimers (Figure 2B), providing new insights into the assembly. The N-terminal helix of the BAX oligomer was found to be highly solvent exposed (Figure S3A) and distant from the main structural domain comprising $\alpha2-\alpha9$. Figure 2C shows that the domain ($\alpha2-\alpha9$) can be further divided into two regions. The top region ($\alpha2-\alpha5$) is highly similar to the structure of the BH3-in-groove model (Czabotar et al., 2013) (a comparison made in Figures S3B and S3C), which was previously reported to be the most important structural feature of an activated BAX (Czabotar et al., 2013; Dewson et al., 2012). The domain ($\alpha2-\alpha5$) forms a symmetric dimer in which $\alpha2$ (the BH3 domain) of each monomer engages $\alpha3-\alpha5$ of the other monomer (Figure 2C). Thus, the dimer is held together by contacts made in both of its BH3-in-groove interfaces. The core structure ($\alpha2-\alpha5$) of our DEER-based result supports the long-standing model for BAX oligomerization that the formation of BAX oligomer proceeds with nucleation of dimers via interactions between BH3 domains (Dewson et al., 2012).

The helical hairpin of $\alpha5-\alpha6$ (Figure 1A) was recently reported to be critical to stabilizing the native structure of the inactive BAX monomer (Bleicken et al., 2014; Chan et al., 2015; Westphal et al., 2014). Our result (Figure 2) indicates that upon oligomerization, the hairpin structure collapses and forms into a clamp-like conformation via a partial opening of $\alpha5-\alpha6$. This finding is consistent with recent studies that support the opening of the hairpin as a critical on-pathway event to the formation of a stabilized apoptotic oligomer at membrane (Bleicken et al., 2014; Westphal et al., 2014). The bottom region, which contains $\alpha6-\alpha9$ (Figure 2C), exhibits some new structural features that have not been reported. The two $\alpha9$ helices are buried within the dimer and stacked above a platform made of $\alpha6-\alpha8$ helices. As $\alpha9$ is characterized by a transmembrane-like helix, this structural arrangement of $\alpha6-\alpha9$ seems critical to removing $\alpha9$ from solvent exposure, explaining why the full-length BAX oligomers can be purified in the absence of lipid membranes. Our result not only reveals a C2 symmetric homodimer in the BAX oligomer whose core structure is akin to the BH3-in-groove model but also unveils the importance of the clamp-like conformation of $\alpha5-\alpha6$, which is implicated in linking the top and bottom parts of the activated dimer. The DEER results provide the structural basis for the formation of soluble BAX oligomers.

Validation of the Interfaces between Active Monomers and Dimers within the Oligomer

To further validate the DEER-derived structural model for the oligomer, we prepared BAX mutants, each monomer carrying one spin label near the interfaces between the assemblies of monomers or dimers. All of the ESR spectra shown (Figure 3) were obtained from purified oligomers of the BAX mutants.

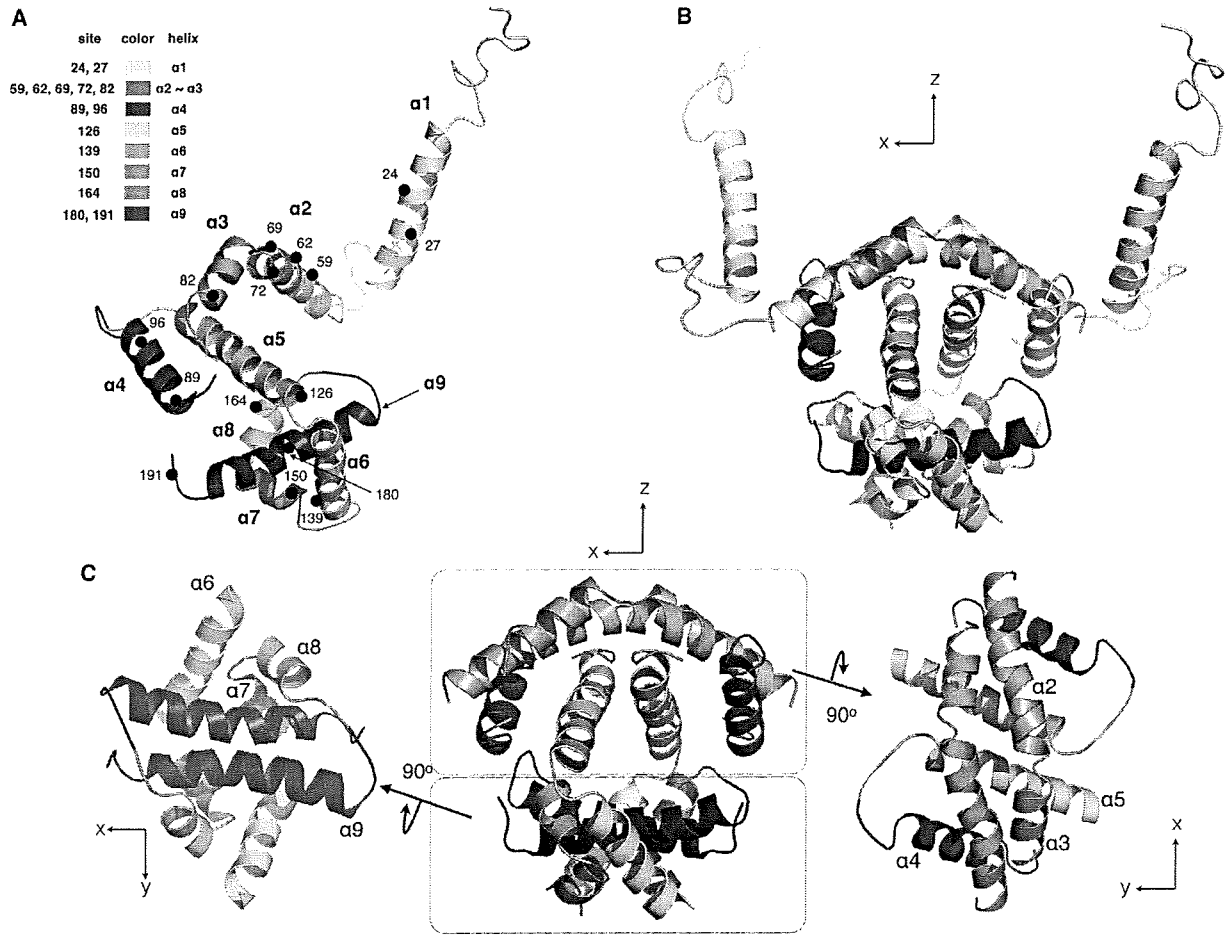

Figure 2. DEER-Derived Structure of Activated BAX Dimer, Which Assembles into an Oligomer

(A) Cartoon structure of activated BAX monomer determined from the DEER results of BAX oligomer study. Spin-labeling sites are denoted by black filled circles.

(B) Cartoon model of BAX dimer structure, in which one BAX is colored according to (A) and the other is colored in pale green.

(C) Cartoon structure of BAX dimer (α1 not shown). Helices are colored according to (A). Top (α2–α5) and bottom (α6–α9) regions of the dimer are zoomed to show local arrangement of the helices. See also Figures S2 and S3.

Continuous wave (cw)-ESR, which is sensitive to detecting interspin distances less than 2 nm, was carried out to validate the interfaces (Chiang et al., 2009; Rabenstein and Shin, 1995). Figure 3A shows the result for the BH3 domain (within α2–α3), in which the inset shows a cartoon of the BH3-in-groove model of the dimer with the spin-labeled sites indicated. The normalized cw-ESR spectra from the indicated sites can be divided into three groups according to the observed linewidth broadening. The lower the peak magnitude of a normalized spectrum, the greater is the dipole-induced linewidth, hence the shorter distances between spin labels (Altenbach et al., 2001; Chiang et al., 2009). The spectra (in black) from the individual sites (62R1, 63R1, 64R1, 65R1, and 67R1) show no sign of linewidth broadening, indicating that the interspin distances are greater than 2 nm. The linewidth of the 66R1 (in red) is among the largest linewidth broadening as the two side chains of the 66R1 are observed to face each other in the dimer structure. The rest of the spectra (69R1, 72R1, and 73R1, shown in blue) exhibit clear linewidth broadening compared with the spectra in black. Sites corresponding to the presence and absence of dipolar broadening are denoted by red and yellow, respectively, in the inset (Figure 3A). The dipole-induced linewidth caused by the contact between BAX was observed to be reduced in a spin dilution experiment (Figure S3D). The cw-ESR results provide strong support for the BH3-in-groove structural model determined from our DEER study.

The same strategy was used to demonstrate the interface in the dimer (Figure 3B). Because the intermonomer distance of 150R1/150R1 is greater than 2.5 nm in the MtsslWizard calculations, the cw-ESR spectrum of 150R1 is used as a reference representing a typical linewidth in the absence of dipolar broadening. All of the other spectra (Figure 3B) exhibit a distinctly greater linewidth broadening compared with the 150R1, indicating that the interspin distances of 66R1/66R1, 96R1/96R1, 114R1/114R1, 180R1/180R1, and 182R1/182R1 are clearly less than 2 nm. The studied sites are highlighted (in red) in the

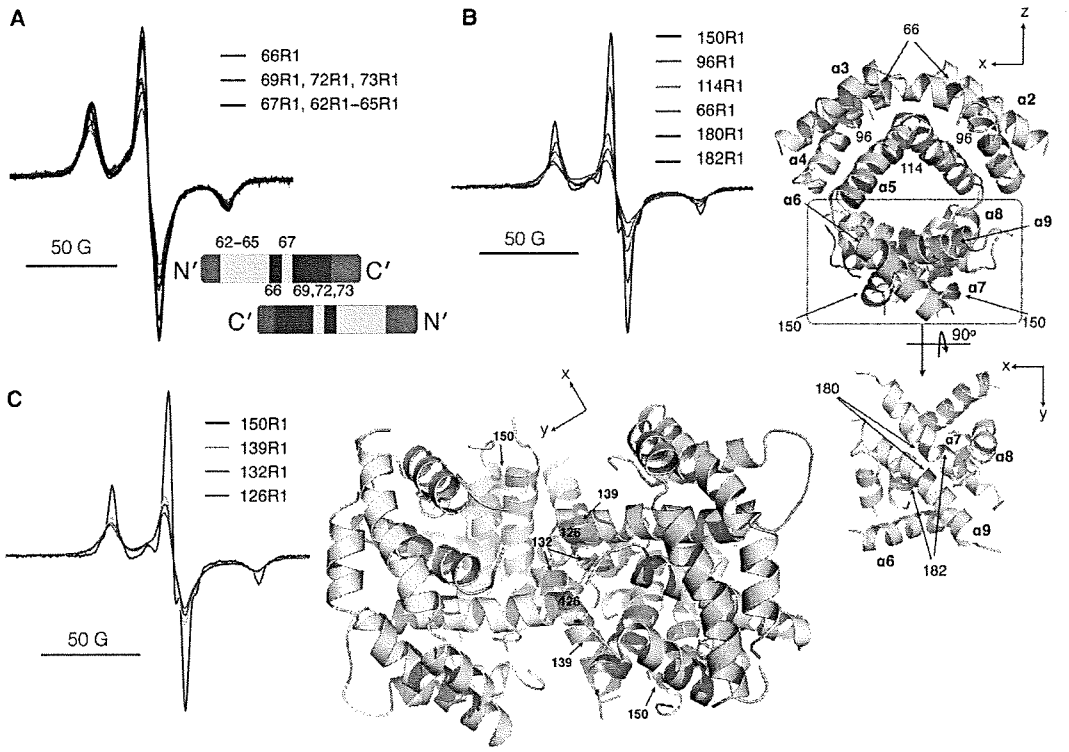

Figure 3. Validation of Monomer and Dimer Interfaces in the Oligomer by cw-ESR

(A) Normalized cw-ESR spectra of oligomer BAX mutants. Side chain of the spin label is denoted by R1. Linewidth broadening is observed to be greater in 66R1 than in 69R1, 72R1, and 73R1. The spectra in black show insignificant linewidth broadening. The inset illustrates the locations of the studied sites in the BH3-in-groove model, agreeing with the DEER-derived model (Figure 2C).

(B) Normalized cw-ESR spectra of oligomer BAX mutants used to study monomer-monomer interface in the dimer. The closer the intermonomer distance in the structural model, the lower the amplitude of normalized spectrum. The dimer is colored (cyan and gray) according to monomer unit. Helices of the monomer unit in cyan are indicated.

(C) Normalized cw-ESR spectra of oligomer BAX mutants used to study dimer-dimer interface in the tetramer shown. The two dimers are coupled via respective monomers (colored cyan and yellow). The indicated sites (126R1, 132R1, and 139R1) are spatially close (<2 nm) at the interface between dimers. Zoom of 139R1 is given (Figure S4). The tetramer model was obtained by seeding the activated BAX monomer in the structural docking using the MtsslWizard and MMM programs. See also Figures S3 and S4.

cartoon structure of the dimer (Figure 3B), showing that they are located at the monomer-monomer interface within the dimer. The distance of 180R1/180R1 is among the shortest. Therefore, its corresponding spectrum displays the lowest magnitude of the central peak among the collected spectra. Although the spatial locations between 182R1/182R1 also appear close in the model, their side chains are pointing away from each other, hence causing an increase in the peak amplitude (i.e., a decrease in the linewidth broadening) of the spectrum compared with the 180R1/180R1 spectrum. The monomer-monomer interface in the DEER-derived dimer is clearly verified using this cw-ESR method.

The same strategy was also used to investigate the dimer-dimer interface within the oligomer (Figure 3C). Again, the spectrum of 150R1 is used as a reference. The spectra of 126R1, 132R1, and 139R1 are clearly broader in linewidth compared with the 150R1, demonstrating their locations at the interface. A structural model of the BAX tetramer is shown (Figure 3C), highlighting the location of the spin-labeled sites. The 126R1 and 132R1 are clearly at the dimer-dimer interface of the tetramer. A zoom of the structure is provided (Figure S4) to show that the side chains of the 139R1 sites are spatially close, which accordingly explains the observed linewidth broadening for 139R1. Both sites 132 and 139 are within helix 6 of BAX. Our finding indicates that the helix 6 and the C-terminal of helix 5 (i.e., site 126) are implicated as the interface linking BAX dimers into higher-order oligomers, consistent with literature studies using biochemical methods (Dewson et al., 2012; Zhang et al., 2010). Our structure-based evidence highlights the importance of helix 6. This finding adds weight to the importance of α5–α6 in stabilizing the structures of the dimer unit and also the oligomer. Collectively, these results evidently support the DEER-derived structural model.

BAX Oligomerization Proceeds Slowly via Dimeric Intermediates

To reveal more details of the oligomerization process, we carried out SEC-FPLC after 5 min, 15 min, 30 min of the incubation of 1:1 spin-labeled BAX monomer (N): BimBH3 peptide. Wild-type BAX was used. The SEC-FPLC result (Figure 4A) shows that BAX

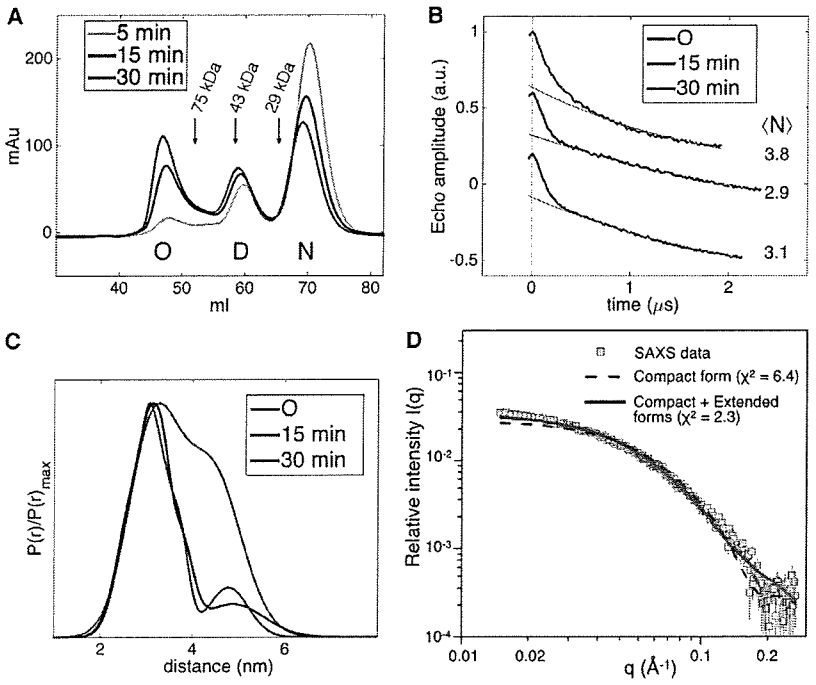

Figure 4. Oligomers Are Assembled From Dimers

(A) SEC-FPLC results after 5-, 15-, and 30-min incubations of wild-type BAX monomers (N) with BimBH3 peptides. N is induced by BimBH3 to transform into dimers (D) and then oligomers (O). Size markers are indicated.

(B) Raw time-domain DEER data. Background traces are shown in grey. The <N> values are shown.

(C) TIKR-P(r) results of the DEER data in (B). The peak around 4.5 nm in the P(r) becomes comparable with the 3-nm peak only when O is present in abundance in the measurements.

(D) SAXS data and modeling fits by EOM approach. χ^2 value of the least-squares fits is improved with 1:3 compact/extended dimer forms (Figure S5). See also Figure S5.

dimers (D) were clearly present after 5 min of the incubation and that as the incubation time was increased from 5 to 15 and 30 min, the amount of D changed little while the amount of the induced BAX oligomers (O) continued increasing over time. The result suggests an important feature of the BAX oligomerization, namely, that oligomerization proceeds slowly in orders of minutes and via nucleation of dimers. DEER measurements were performed for the incubations corresponding to 15 min and 30 min. The DEER results (Figures 4B and 4C) were plotted together with the result of the purified wild-type oligomers (i.e., the 62/126-R1 oligomers, shown in Figures 1 and S1A). The modulation depth of the DEER data was analyzed to yield the number <N> of coupled spins (see Figure 4B). The <N> values were between 2.9 and 3.1 for the incubations of 15 min and 30 min, showing an increase with the incubation time. A dominant peak at distances around 3 ± 0.8 nm in the P(r) results was observed in all of the three measurements, in accordance with our structural model (Figures 1 and 2) and literature data (Bleicken et al., 2014; Tsai et al., 2015) that the intramonomer distances between 62R1 and 126R1 remain in the range of 2–4 nm, before and after the oligomerization. There are clear differences in the P(r) between the purified oligomer and the incubations of 15 min and 30 min. A peak at longer distances (ca. 4.5 ± 0.3 nm, Figure 4C) was observed to be weak in the 15- and 30-min incubations, whereas it became relatively stronger in the result of the purified oligomers. Our structural model and the modeling calculations (cf. 62/126-R1 in Figure S2C) indicate that the 4.5-nm peak is mainly caused by the intermonomer distances within the oligomer. It is thus reasonable to observe a relatively weak peak around 4.5 nm in the 15-min and 30-min incubations (Figure 4C) because the amount of the O is clearly less than 30% of the total amount of BAX (including O, D, and N, shown in Figure 4A) in those measurements.

To further confirm the existence of the dimer forms during oligomerization, we performed a SAXS experiment together with online high-performance liquid chromatography (HPLC) (Figure S5A) and analyzed the data to characterize the solution structure of the dimers using the ensemble optimization method (EOM) (Bernadó et al., 2007). The preparation of the BAX dimers that correspond to intermediates between the N and O is given in Supplemental Experimental Procedures. SAXS data (Figure 4D) of the dimer fractions from HPLC can be fitted reasonably well with the ensemble structures selected from a pool of compact and extended dimer forms (with a ratio of 1:3; Figure S5B), but somewhat less satisfactorily with a pool consisting of only the compact form (i.e., the dimer model derived from the DEER measurements of the purified BAX O, shown in Figure 2B). Since the eluted samples from HPLC in the SAXS measurement represent intermediate states between N and O, the introduction of a hypothetical intermediate structure (i.e., the extended form, characterized by a similar but more loose structure as opposed to the compact D form; Figures S5C and S5D) is necessary to achieve a satisfactory fit to the SAXS data. This SAXS study demonstrates the structural similarity between the intermediate and the final (i.e., the dimer within BAX O) states of BAX dimer, establishing a correspondence between the two states. Moreover, it provides additional evidence supporting the DEER-derived structure.

Apoptotic Activity of the Soluble BAX O

Below, we demonstrate that the soluble BAX oligomers retain the functional activity of BAX for inducing MOMP and releasing cytochrome *c* from mitochondria. Unless indicated, all BAX used in the experiments shown in Figure 5 were wild-type (WT) BAX. The result of the cytochrome *c* release experiments shows that (Figure 5A) N is of low cytochrome *c* release efficiency, suggesting that N is mostly inactive and cytosolic, thereby playing an insignificant role in inducing MOMP. The highest efficiency to promote the release of cytochrome *c* was observed with O, which is known to effectively permeabilize the outer mitochondrial membranes. The oligomer of BAX mutants ($O^{126/164}$) was

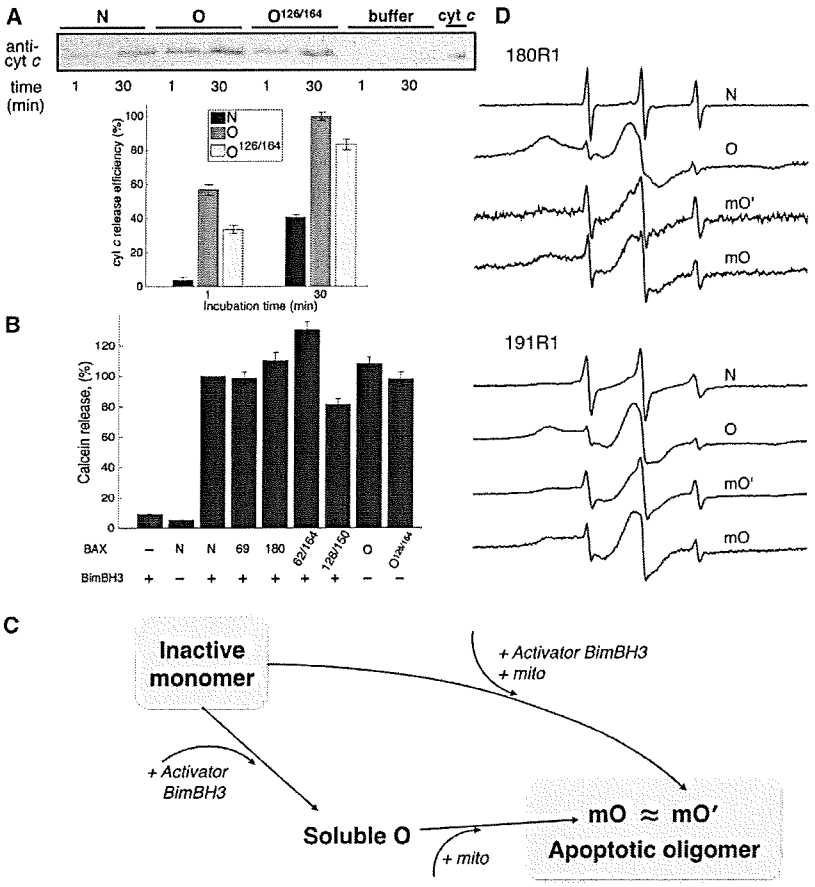

Figure 5. Apoptotic Activity and Membrane Insertion of BAX

(A) Cytochrome *c* (cyt c) release from mitochondria (mito) on incubation of BAX proteins as a function of the incubation time. Buffer without BAX proteins was used as a negative control.

(B) Calcein release assay from PC/CL vesicles with WT BAX monomers (N), oligomers (O), and other cysteine variants of BAX as indicated. Data are normalized to +/+ (N/BimBH3). Controls for −/+ and +/− are given. Only in the presence of BimBH3 can the BAX monomers (WT, 69, 180, 62/164, and 126/150) be activated to cause a large release of calcein from the vesicles. Otherwise, soluble BAX O must be used to cause the release.

(C) A proposed model that inactive cytosolic BAX can be activated to become membrane-associated oligomer via two different pathways. Both the mO and mO′ are demonstrated to have the ability to induce MOMP.

(D) cw-ESR spectra of 180R1 and 191R1, measured at 300 K (field width: 100 G) in the states of soluble N, soluble O, mO′, and mO.

The estimation of errors is based on at least three independent measurements.

observed to release cytochrome *c* with slightly less efficiency compared with the result of O. A control using cytochrome *c* was also shown. These in vitro assays demonstrate the MOMP ability of the soluble BAX O, suggesting an important role of the soluble oligomers in initiating apoptosis in cells. Moreover, calcein release assay was also performed (Figure 5B) to verify that even in the absence of other membrane proteins (e.g., other Bcl2 family members) from mitochondria, our recombinant mutants retained the membrane-permeabilizing activity. These results demonstrate that the soluble BAX O has the ability to induce MOMP.

Association of Soluble Oligomers with Membrane

Despite extensive study, the structures of the membrane-embedded BAX oligomer remain contentious. The present study proposes (Figure 5C) that BAX can convert from inactive (cytosolic) monomer to active (membrane-embedded) oligomers via two different pathways. That is, the active membrane-embedded oligomer could exist in two forms, but differences in the structure and apoptotic function of the two forms seem insignificant, as detailed below. One is formed from BAX monomers in the presence of BH3 activators (e.g., BimBH3) and membrane lipids and the other is formed from soluble O in the presence of membrane lipids; hereafter, they are designated as mO′ and mO, respectively. Most of the previous studies have focused on determining structures of the dimeric segments containing helices α2–α3 or α5–α6 in membrane environments (i.e., the mO′); a clear picture of the complete complex (α1–α9) is still lacking. Our structural model, although based on soluble oligomers, is consistent with the reported models for mO′ in the helices 2–6 (Bleicken et al., 2014; Czabotar et al., 2013; Westphal et al., 2014). Given that (1) both the mO and mO′ are verified (in the present study) to act as apoptotic oligomers and (2) the α2–α6 domain of the soluble O is structurally similar to that of the mO′, it is, therefore, reasonable to presume that some changes in the C-terminal region are needed for the soluble O to convert into the mO.

We carried out cw-ESR to investigate the local environment of the C-terminal helix. BAX mutants, carrying spin label at either 180 or 191 within helix 9, were prepared to obtain spectra for the N, O, mO, and mO′ states, where the latter two were from the pellets of the incubations of soluble O and N, respectively, in the presence of mitochondria (mito) (see Supplemental Experimental Procedures). Because the C terminus is buried inside the soluble O (Figures 2 and 3), cw-ESR spectra of the two BAX O mutants were observed to be highly immobilized compared with the spectra of the inactive, cytosolic BAX N (Figure 5D). The immobilized linewidth was found to be clearly reduced in the states of mO and mO′, verifying that upon association of the soluble O with mitochondria, the conformation of the C-terminal helices is adapted for the conversion into mO. The spectra of either mutant are similar between the mO and mO′ states, indicating that the local environments of helix 9 are comparable between the two states. It suggests that there is only modest difference between the C-terminal conformations of the mO and mO′. An alternative pathway for the BAX activation to convert

from monomers into soluble O (in the absence of membrane lipids), followed by the integration into membrane to form the mO, is thus proposed (Figure 5C).

DISCUSSION

Activation of cytosolic BAX proteins is a fundamental determinant for the initiation of mitochondria-mediated apoptosis. During the apoptosis, BAX undergoes dramatic conformational changes to unfold and form a membrane-associated complex, but how the activated BAX oligomer is assembled from inactive monomers has been poorly understood. Here, we present a solution structural model of the activated BAX oligomer, showing that the oligomer is assembled from homodimers. The determined structure reveals details of the assemblies of the BH3-in-groove dimer and supports the opening of the hairpin formed by helices 5–6 in the oligomer state. Helices 5–6 were verified to play an important role in both stabilizing the dimer unit and linking the dimers into higher-order oligomers, establishing the dimer-dimer interface in the oligomer. This finding about helices 5–6 provides explanation for a recent study that BAX oligomerization could be inhibited by introducing a 21-residue vMIA peptide that contacts BAX and stabilizes helices 5–6 (Ma et al., 2012). Moreover, our study reveals that in the soluble O state, helix 1 is highly flexible and solvent exposed while helix 9 is buried within the soluble O. Upon incubation of the soluble O with mitochondria, helix 9 was found to insert into the membranes, whereas the local environment of helix 1 changed little and remained highly exposed. The finding about helix 1 is reasonable as the region (residues 12–24 of BAX) is known to be the target of monoclonal antibody, 6A7, requiring the N terminus to remain highly exposed in the activated state (Hsu and Youle, 1998).

The role of helix α9 in regulating BAX-mediated apoptosis has been a long-standing puzzle. It was shown that C-terminal truncated BAX (BaxΔC) could still cause membrane insertion and permeabilization, suggesting that the absence of α9 did not impair the ability of BAX to induce MOMP (Antonsson et al., 2001); the BaxΔC was also shown to have almost the same activity as full-length BAX when expressed in neurons. On the contrary, studies made with GFP-fused BAX proteins showed that the absence of α9 prevented the ability of the fusion protein to be translocated to mitochondria after an apoptotic signal (Nechushtan et al., 1999). Experiments made on isolated mitochondria showed that, while inactive full-length BAX was not able to cause membrane insertion, a chimeric protein formed of BaxΔC fused to the C terminus of Bcl-xL was inserted. Conversely, while Bcl-xL was inserted, a chimeric protein formed of Bcl-xLΔC and the C terminus of BAX was not (Tremblais et al., 1999). This suggests that, unlike the C terminus of Bcl-xL, which is a true transmembrane anchor, the C terminus of BAX is not (Renault and Manon, 2011). The exposure of α9 alone is not adequate to drive the membrane insertion of an activated BAX, unless the key residue (e.g., Thr174 or Ser184, located in the middle of α9) is deleted or phosphorylated to modulate conformations of BAX (Arokium et al., 2004; Nechushtan et al., 1999; Xin et al., 2014). These previous studies suggested that α9 is nearly a transmembrane anchor, but that it requires a significant conformational change to be able to act as such. This present study has revealed molecular details of the conformational changes that are required to make soluble O prone to associate with lipid membrane. It suggests that the formation of soluble O is likely a direct consequence of the BimBH3-induced conformational changes, followed by the integration of the BAX O into membrane.

Very recently, a dimer model of membrane-embedded BAX was proposed, also based on the measurements of DEER spectroscopy (Bleicken et al., 2014). The reported structure (cf. Figure 4C in Bleicken et al., 2014) is consistent with ours in the conformation of the core helices 2–6. Because of complexity in the DEER signals when obtained in membrane environment, a clear picture for the conformations of helices 7–9 and helix 1 was not presented in the study. The present study has made important progress in elucidating the structure of the apoptotic BAX oligomer. Given the improvements in the analysis of DEER measurements by the newly developed methodology (see Supplemental Experimental Procedures), we were able to carry out peak assignments and verification for the TIKR-P(r) results and thus construct a clear model for the solution structures of BAX dimer and tetramer. The formation of BAX oligomers can occur before or upon interaction with membranes, and the two membrane-inserted oligomers, although resulting from two different pathways, are largely similar in structure and have the same ability to induce MOMP.

A solution structure of the BAX oligomer is presented based on these findings. The structure was rigorously derived from the results of the ESR and SAXS measurements as well as molecular modeling. Interfaces between monomers and dimers in the BAX O were carefully verified, providing structural information for developing a therapeutic intervention of apoptosis. Moreover, we showed that the soluble BAX O can convert directly into a membrane-inserted oligomer (i.e., mO), which in turn leads to MOMP and apoptosis, and has several structural characteristics similar to the mO′. Major changes involved in forming the mO from the soluble O occur in the C-terminal region. Although a complete structural model for the mO is yet to be elucidated, our finding has drawn attention to the role of soluble BAX O in regulating apoptosis; this is a point that had never been adequately considered before the present study. This study suggests that the formation of BAX oligomers could occur prior to insertion into mitochondria.

EXPERIMENTAL PROCEDURES

Recombinant Protein Expression and Purification

Unless specified otherwise, all chemicals used in this study were from Sigma-Aldrich. Methanethiosulfonate spin label (MTSSL; 1-oxy-2,2,5,5-tetramethyl-3-pyrroline-3-methyl) (Alexis Biochemicals) was used for spin-labeling study. BimBH3 peptides (Gavathiotis et al., 2008; Tsai et al., 2015) were custom-synthesized by Genomics BioSci & Tech with purity greater than 95%. The sequence of the peptide is (from N to C terminals) DMRPEIWIAQELRRIGDEFNAYYAR. Peptides were further purified by reverse-phase HPLC. Full-length BAX and mutants were prepared as previously described (Chan et al., 2015; Tsai et al., 2015). For spin-labeling study, recombinant BAX mutants of this study were prepared using a QuikChange mutagenesis kit (Stratagene) to bear only two or one cysteine residues at the indicated sites. A typical yield (>95% purity) of 0.15 mg/l culture could reproducibly be obtained for WT BAX. For cysteine variants of BAX, typical yield (>95% purity) was 0.15 mg to 0.05 mg/l. WT BAX carries two endogenous cysteine residues at sites 62 and 126; it is denoted by WT BAX-R1 or 62/126R1

if the two cysteine sites are conjugated with the MTSSL probe to form two R1 side chains. Proteins/peptides were labeled with a 10-fold excess of the MTSSL label per cysteine residue overnight (>12 hr) in the dark at 277 K. To remove free radicals, the spin-labeled BAX solution was dialyzed against four changes of buffer A (20 mM sodium phosphate [pH 8.0], 100 mM NaCl) over 1–3 hr and final change of buffer over 24 hr. Volume of the buffer was about 1,000 times that of the protein solution. MALDI-TOF experiments were conducted to confirm the identity of the peptides/proteins carrying the spin labels. Spin dilution was carried out with 1:1 labeled/unlabeled BAX. All of the DEER measurements of doubly labeled BAX oligomers (Figure 1E) were performed with spin dilution to reduce dipolar couplings between BAX monomers.

Activation of BAX by BimBH3

BAX monomer was activated to become apoptotic by incubation with 4-fold molar concentration of BimBH3 peptide at room temperature for >6 hr, in buffer B (20 mM sodium phosphate [pH 8.0], 100 mM NaCl, and 0.5% zwitterionic detergent, CHAPS). The length of the incubation time (>6 hr) was determined based on our previous time-resolved ESR study that showed that the reaction of the BimBH3-induced BAX oligomerization required more than 6 hr to finish (Tsai et al., 2015). CHAPS is a frequently used detergent in BAX purification, because unlike most other detergents (e.g., octylglucoside and Triton X-100), it does not provoke inactive BAX to oligomerize (Antonsson et al., 2000; Bleicken et al., 2010; Yao et al., 2014). The addition of CHAPS was to increase the solubility of the apoptotic oligomers during the incubation with BimBH3. More than 10% increase in the yield of BAX O was observed with the addition of 0.5% CHAPS in the activation buffer. Activated BAX proteins were separated with SEC using a HiLoad 16/60 Superdex 75 column (GE Healthcare) with the buffer A containing no CHAPS. The chromatogram demonstrated monomeric fractions at ~70 ml, dimeric fractions at ~60 ml, and oligomeric fractions approximately within 45–50 ml, as described previously (Tsai et al., 2015). The molecular weight of the oligomer is approximately 440 kDa, consistent with the previous studies (Bleicken et al., 2010). The eluded oligomeric fractions were thus taken as soluble BAX oligomers because the concentration of CHAPS in the buffer during the FPLC purification was far below the critical micelle concentration of CHAPS. Our results verified that CHAPS caused insignificant changes to BAX and that the presence of CHAPS did not induce BAX oligomerization (Figure S1B).

For the mO preparation, soluble BAX O was incubated with mitochondria for 30 min at 303 K water bath. For the mO′ preparation, BAX monomer:BimBH3 1:4 was incubated with mitochondria for 60 min at 303 K water bath. After incubation, samples were centrifuged and the resulting pellets were collected for ESR experiment. The spectra from the mO and mO′ were re-collected after 12 hr incubation to confirm that they changed insignificantly over time. The final concentration of spin-labeled BAX was ca. 0.3 mM.

Pulsed/cw-ESR Experiments, TIKR Analysis, and Molecular Modeling

Approximately, 40 μl solution volume, containing 30% (v/v) d8-glycerol as cryoprotectant, was added into a quartz ESR tube. All buffers in the DEER experiments were deuterated. Concentration of BAX in ESR measurements was ca. 0.3–0.5 mM. A Bruker ELEXSYS E580-400 cw/pulsed spectrometer, with a dielectric resonator (ER4118X-MD5W) and a helium gas flow system (4118CF and 4112HV), was used. The cw-ESR experiment was performed at an operating frequency of 9.4 GHz and 1.5 mW incident microwave power. The swept magnetic range was 200 Gauss. The ESR probehead was pre-cooled to a desired temperature prior to the transfer of the ESR sample tube into the cavity. Equilibrium time was 20 min for each temperature variation. All of the cw-ESR spectra used for the determination of interfaces between BAX monomers and dimers (Figure 3) were obtained at 200 K, a commonly used temperature that is low enough so that the motion of interspin vectors is sufficiently slow not to average the major dipolar anisotropy (Chiang et al., 2009; Rabenstein and Shin, 1995).

DEER experiments were carried out using the typical four-pulse constant-time DEER sequence, as previously described (Huang et al., 2011; Milov et al., 1984; Pannier et al., 2000; Tsai et al., 2015). The detection pulses were set to 32 ns and 16 ns for π and $\pi/2$ pulses, respectively, and pump frequency was set to approximately 70 MHz lower than the detection pulse frequency. The pulse amplitudes were chosen to optimize the refocused echo. The $\pi/2$-pulse was used with +x/–x phase cycle to eliminate receiver offsets. The duration of pumping pulse was about 32 ns, and its frequency was coupled into the microwave bridge by a commercially available setup (E580-400U) from Bruker. All pulses were amplified via a pulsed traveling wave tube amplifier (E580-1,030). The field was adjusted so that the pump pulse is applied to the maximum of the nitroxide spectrum, where it selects the central $m_I = 0$ transition of Azz together with the $m_I = \pm 1$ transitions. A common cooling approach was used (Georgieva et al., 2012). The sample tube was plunge-cooled in liquid nitrogen and then transferred into the ESR probehead, which was pre-cooled to 50 K using the helium flow system. The procedure was generally used to kinetically trap the structural properties of a protein in a room temperature state. Accumulation time for each set of data was 10–18 hr at 50 K.

Determination of interspin distance distribution P(r) from DEER experiments was performed in the time-domain analysis by TIKR based on the L-curve method (Chiang et al., 2005), herein called the TIKR method. When the TIKR-P(r) obtained displayed a heterogeneity-like distribution, a Gaussian-based method was used to verify the heterogeneity, as described in the following section. Moreover, TIKR distances and distributions were checked against modeled distances for spin-label rotamers attached to the protein structures (Figures 1 and 2). The modeled intramonomer and intermonomer distances were obtained using the program MtsslWizard (Hagelueken et al., 2012), which operates as a plugin of the PyMOL. MtsslWizard searches for ensembles of possible MTSSL rotamers that do not clash with a static model of the protein. The program contains a sub-program called MtsslDock (Hagelueken et al., 2012, 2013), which allows the user to dock two macromolecules based on a set of intermolecular distances obtained from DEER measurements. MtsslDock uses a mixed genetic and evolutionary algorithm to find docking models between two macromolecules (e.g., two BAX monomers or two BAX dimers) that agree with the experimental distance data. This MtsslWizard program (including MtsslDock) has been evaluated in a number of challenging studies and it has been shown to predict experimental data well (Hagelueken et al., 2012, 2013). The benefits of the program are its accuracy and simplicity.

Moreover, an MMM software package (Polyhach et al., 2011) was also used to produce MMM-P(r) distance distributions to confirm the distances from the MtsslWizard calculations and the TIKR-P(r) results. The MMM software was developed to determine the interspin-label distances and distributions based on the analysis of spin-label rotamers. Distance distributions from the oligomers of the spin-labeled BAX mutants were predicted with rotamer library modeling of MTSSL conformations using MMM (version 2013). The rotamer library was previously obtained by iterative projection of a long molecular dynamics trajectory of the free spin label onto a set of canonical dihedral angles and shown to provide a good representation of the underlying trajectory adequate for ESR distance measurements. In the present study, both the MMM and MtsslWizard were used to verify the structural models derived from the TIKR results.

SUPPLEMENTAL INFORMATION

Supplemental Information includes Supplemental Experimental Procedures, five figures, and one table and can be found with this article online at http://dx.doi.org/10.1016/j.str.2015.07.013.

AUTHOR CONTRIBUTIONS

Y.W.C. and T.C.S. designed research, analyzed data, and wrote the paper. T.C.S., C.Y.L., Y.C.L., and C.L.H. performed the research. O.S., Y.Q.Y., and S.L. performed the SAXS study. All authors discussed the results.

ACKNOWLEDGMENTS

This work was supported by the Ministry of Science and Technology of Taiwan (102-2628-M-007-003-MY3 and 103-2627-M-007-005). All of the cw/pulse ESR measurements were conducted in the Research Instrument Center of Taiwan located at NTHU.

Received: April 13, 2015
Revised: July 6, 2015
Accepted: July 28, 2015
Published: August 20, 2015

REFERENCES

Airola, M.V., Sukomon, N., Samanta, D., Borbat, P.P., Freed, J.H., Watts, K.J., and Crane, B.R. (2013). HAMP domain conformers that propagate opposite signals in bacterial chemoreceptors. PLoS Biol. *11*, e1001479.

Altenbach, C., Oh, K.J., Trabanino, R.J., Hideg, K., and Hubbell, W.L. (2001). Estimation of inter-residue distances in spin labeled proteins at physiological temperatures: experimental strategies and practical limitations. Biochemistry *40*, 15471–15482.

Antonsson, B., Montessuit, S., Lauper, S., Eskes, R., and Martinou, J.C. (2000). Bax oligomerization is required for channel-forming activity in liposomes and to trigger cytochrome c release from mitochondria. Biochem. J. *345*, 271–278.

Antonsson, B., Montessuit, S., Sanchez, B., and Martinou, J.C. (2001). Bax is present as a high molecular weight oligomer/complex in the mitochondrial membrane of apoptotic cells. J. Biol. Chem. *276*, 11615–11623.

Arokium, H., Camougrand, N., Vallette, F.M., and Manon, S. (2004). Studies of the interaction of substituted mutants of BAX with yeast mitochondria reveal that the C-terminal hydrophobic alpha-helix is a second ART sequence and plays a role in the interaction with anti-apoptotic BCL-xL. J. Biol. Chem. *279*, 52566–52573.

Bernadó, P., Mylonas, E., Petoukhov, M.V., Blackledge, M., and Svergun, D.I. (2007). Structural characterization of flexible proteins using small-angle X-ray scattering. J. Am. Chem. Soc. *129*, 5656–5664.

Bleicken, S., Classen, M., Padmavathi, P.V.L., Ishikawa, T., Zeth, K., Steinhoff, H.J., and Bordignon, E. (2010). Molecular details of Bax activation, oligomerization, and membrane insertion. J. Biol. Chem. *285*, 6636–6647.

Bleicken, S., Jeschke, G., Stegmueller, C., Salvador-Gallego, R., García-Sáez, A.J., and Bordignon, E. (2014). Structural model of active Bax at the membrane. Mol. Cell *56*, 496–505.

Bode, B.E., Margraf, D., Plackmeyer, J., Durner, G., Prisner, T.F., and Schiemann, O. (2007). Counting the monomers in nanometer-sized oligomers by pulsed electron-electron double resonance. J. Am. Chem. Soc. *129*, 6736–6745.

Cartron, P.-F., Bellot, G., Oliver, L., Grandier-Vazeille, X., Manon, S., and Vallette, F.M. (2008). Bax inserts into the mitochondrial outer membrane by different mechanisms. FEBS Lett. *582*, 3045–3051.

Chan, C.-H., Tsai, C.-J., and Chiang, Y.-W. (2015). Side-chain packing interactions stabilize an intermediate of BAX protein against chemical and thermal denaturation. J. Phys. Chem. B *119*, 54–64.

Chiang, Y.W., Borbat, P.P., and Freed, J.H. (2005). The determination of pair distance distributions by pulsed ESR using Tikhonov regularization. J. Magn. Reson. *172*, 279–295.

Chiang, Y.W., Zheng, T.Y., Kao, C.J., and Horng, J.C. (2009). Determination of interspin distance distributions by cw-ESR is a single linear inverse problem. Biophys. J. *97*, 930–936.

Czabotar, P.E., Westphal, D., Dewson, G., Ma, S., Hockings, C., Fairlie, W.D., Lee, E.F., Yao, S.G., Robin, A.Y., Smith, B.J., et al. (2013). Bax crystal structures reveal how BH3 domains activate bax and nucleate its oligomerization to induce apoptosis. Cell *152*, 519–531.

Dejean, L.M., Martinez-Caballero, S., Guo, L., Hughes, C., Teijido, O., Ducret, T., Ichas, F., Korsmeyer, S.J., Antonsson, B., Jonas, E.A., et al. (2005). Oligomeric Bax is a component of the putative cytochrome c release channel MAC, mitochondrial apoptosis-induced channel. Mol. Biol. Cell *16*, 2424–2432.

Dewson, G., Ma, S., Frederick, P., Hockings, C., Tan, I., Kratina, T., and Kluck, R.M. (2012). Bax dimerizes via a symmetric BH3:groove interface during apoptosis. Cell Death Differ. *19*, 661–670.

Gavathiotis, E., Suzuki, M., Davis, M.L., Pitter, K., Bird, G.H., Katz, S.G., Tu, H.C., Kim, H., Cheng, E.H.Y., Tjandra, N., et al. (2008). BAX activation is initiated at a novel interaction site. Nature *455*, 1076–1081.

Gavathiotis, E., Reyna, D.E., Davis, M.L., Bird, G.H., and Walensky, L.D. (2010). BH3-triggered structural reorganization drives the activation of proapoptotic BAX. Mol. Cell *40*, 481–492.

Georgieva, E.R., Roy, A.S., Grigoryants, V.M., Borbat, P.P., Earle, K.A., Scholes, C.P., and Freed, J.H. (2012). Effect of freezing conditions on distances and their distributions derived from double electron electron resonance (DEER): a study of doubly-spin-labeled T4 lysozyme. J. Magn. Reson. *216*, 69–77.

Georgieva, E.R., Borbat, P.P., Ginter, C., Freed, J.H., and Boudker, O. (2013). Conformational ensemble of the sodium-coupled aspartate transporter. Nat. Struct. Mol. Biol. *20*, 215–221.

Häcker, G., and Weber, A. (2007). BH3-only proteins trigger cytochrome c release, but how? Arch. Biochem. Biophys. *462*, 150–155.

Hagelueken, G., Ward, R., Naismith, J.H., and Schiemann, O. (2012). MtsslWizard: in silico spin-labeling and generation of distance distributions in PyMOL. Appl. Magn. Reson. *42*, 377–391.

Hagelueken, G., Abdullin, D., Ward, R., and Schiemann, O. (2013). mtsslSuite: in silico spin labelling, trilateration and distance-constrained rigid body docking in PyMOL. Mol. Phys. *111*, 2757–2766.

Hsu, Y.-T., and Youle, R.J. (1998). Bax in murine thymus is a soluble monomeric protein that displays differential detergent-induced conformations. J. Biol. Chem. *273*, 10777–10783.

Huang, Y.W., Lai, Y.C., Tsai, C.J., and Chiang, Y.W. (2011). Mesopores provide an amorphous state suitable for studying biomolecular structures at cryogenic temperatures. Proc. Natl. Acad. Sci. USA *108*, 14145–14150.

Jeschke, G. (2012). DEER distance measurements on proteins. Annu. Rev. Phys. Chem. *63*, 419–446.

López, C.J., Yang, Z., Altenbach, C., and Hubbell, W.L. (2013). Conformational selection and adaptation to ligand binding in T4 lysozyme cavity mutants. Proc. Natl. Acad. Sci. USA *110*, E4306–E4315.

Ma, J., Edlich, F., Bermejo, G.A., Norris, K.L., Youle, R.J., and Tjandra, N. (2012). Structural mechanism of Bax inhibition by cytomegalovirus protein vMIA. Proc. Natl. Acad. Sci. USA *109*, 20901–20906.

Milov, A.D., Ponomarev, A.B., and Tsvetkov, Y.D. (1984). Electron electron double-resonance in electron-spin echo–model biradical systems and the sensitized photolysis of decalin. Chem. Phys. Lett. *110*, 67–72.

Moldoveanu, T., Follis, A.V., Kriwacki, R.W., and Green, D.R. (2014). Many players in BCL-2 family affairs. Trends Biochem. Sci. *39*, 101–111.

Nechushtan, A., Smith, C.L., Hsu, Y.T., and Youle, R.J. (1999). Conformation of the Bax C-terminus regulates subcellular location and cell death. EMBO J. *18*, 2330–2341.

Pannier, M., Veit, S., Godt, A., Jeschke, G., and Spiess, H.W. (2000). Dead-time free measurement of dipole-dipole interactions between electron spins. J. Magn. Reson. *142*, 331–340.

Pliotas, C., Ward, R., Branigan, E., Rasmussen, A., Hagelueken, G., Huang, H., Black, S.S., Booth, I.R., Schiemann, O., and Naismith, J.H. (2012). Conformational state of the MscS mechanosensitive channel in solution revealed by pulsed electron-electron double resonance (PELDOR) spectroscopy. Proc. Natl. Acad. Sci. USA *109*, E2675–E2682.

Polyhach, Y., Bordignon, E., and Jeschke, G. (2011). Rotamer libraries of spin labelled cysteines for protein studies. Phys. Chem. Chem. Phys. *13*, 2356–2366.

Rabenstein, M.D., and Shin, Y.K. (1995). Determination of the distance between two spin labels attached to a macromolecule. Proc. Natl. Acad. Sci. USA *92*, 8239–8243.

Renault, T.T., and Manon, S. (2011). Bax: addressed to kill. Biochimie *93*, 1379–1391.

Suzuki, M., Youle, R.J., and Tjandra, N. (2000). Structure of Bax: coregulation of dimer formation and intracellular localization. Cell *103*, 645–654.

Tremblais, K., Oliver, L., Juin, P., Le Cabellec, T.M., Meflah, K., and Vallette, F.M. (1999). The C-terminus of bax is not a membrane addressing/anchoring signal. Biochem. Biophys. Res. Commun. *260*, 582–591.

Tsai, C.-J., Liu, S., Hung, C.-L., Jhong, S.-R., Sung, T.-C., and Chiang, Y.-W. (2015). BAX-induced apoptosis can be initiated through a conformational selection mechanism. Structure *23*, 139–148.

Westphal, D., Dewson, G., Menard, M., Frederick, P., Iyer, S., Bartolo, R., Gibson, L., Czabotar, P.E., Smith, B.J., Adams, J.M., et al. (2014). Apoptotic pore formation is associated with in-plane insertion of Bak or Bax central helices into the mitochondrial outer membrane. Proc. Natl. Acad. Sci. USA *111*, E4076–E4085.

Xin, M., Li, R., Xie, M., Park, D., Owonikoko, T.K., Sica, G.L., Corsino, P.E., Zhou, J., Ding, C., White, M.A., et al. (2014). Small-molecule Bax agonists for cancer therapy. Nat. Commun. *5*, 4935.

Yao, S., Westphal, D., Babon, J.J., Thompson, G.V., Robin, A.Y., Adams, J.M., Colman, P.M., and Czabotar, P.E. (2014). NMR studies of interactions between Bax and BH3 domain-containing peptides in the absence and presence of CHAPS. Arch. Biochem. Biophys. *545*, 33–43.

Youle, R.J., and Strasser, A. (2008). The BCL-2 protein family: opposing activities that mediate cell death. Nat. Rev. Mol. Cell Biol. *9*, 47–59.

Zhang, Z., Zhu, W., Lapolla, S.M., Miao, Y., Shao, Y., Falcone, M., Boreham, D., McFarlane, N., Ding, J., Johnson, A.E., et al. (2010). Bax forms an oligomer via separate, yet interdependent, surfaces. J. Biol. Chem. *285*, 17614–17627.

 ©2015 Elsevier Ltd All rights reserved